



Effect of Solids Content and Spray-Drying Operating Conditions on the Carotenoids Microencapsulation from Pressed Palm Fiber Oil Extracted with Supercritical CO₂

Paula Andrea Osorio Carmona¹ · Lorena Costa Garcia¹ · José Antônio de Aquino Ribeiro¹ · Leonardo Fonseca Valadares¹ · Adriano de Figueiredo Marçal² · Luiz Ferreira de França² · Simone Mendonça¹

Received: 13 April 2018 / Accepted: 11 June 2018 / Published online: 23 June 2018

© Springer Science+Business Media, LLC, part of Springer Nature 2018

Abstract

Carotenoids were extracted from pressed palm fiber using supercritical CO₂ and microencapsulated by spray-drying with gum Arabic. Twenty-eight tests were made. Emulsions were characterized with respect to droplet size and viscosity. The effects of solid content and spray-drying conditions on moisture, hygroscopicity, microencapsulation efficiency, and powder lipid oxidation were investigated. Particles produced at optimized process (35% of solids, feed flow of 26%, temperature of 166 °C, and atomization air flow of 40 mm) were evaluated for major carotenoids identification and fatty acid profile. Higher solid content led to higher encapsulation efficiency and lower lipid oxidation, which was related to the higher emulsion viscosity and lower droplet size. Increasing atomization air flow and temperature resulted in higher lipid oxidation. Moisture increased and hygroscopicity decreased when higher feed flow and lower temperature were used. Microparticles presented high content of monounsaturated fatty acids, α -, β -, and (9Z)- β -carotene and reflected the composition of un-encapsulated oil.

Keywords Pressed palm fiber oil · Carotenoids · Emulsion properties · Microencapsulation efficiency · Peroxide value · Spray dryer parameters

Introduction

In recent years, there is an increasing public interest in sustainable development as response to environmental pollution problems caused by industrial activities and economic development (Cardenas-Toro et al. 2014, and Singla et al. 2018). Palm oil (*Elaeis guineensis* Jacq.) is one of the highly significant industrial crops because of its importance to vegetable oil production for cooking, cosmetics, pharmaceutical compounds, and biofuels production. However, with planting area growth, the palm oil industry is generating large quantities of

waste, with an estimated amount of 184 million tons annually in the world (Vakili et al. 2015). Pressed palm fiber (PPF), a residue obtained after fruit mesocarp extraction and generally used as fuel for energy generation, represents approximately 12% of processed fresh fruit bunch (Rosa et al. 2011). PPF also contains an oil constituted by a mixture of triacylglycerols and high content of natural antioxidants, such as vitamin E and carotenoids, especially α - and β -carotene, both precursors of vitamin A (Sambanthamurthiilva et al. 2000).

The main constituents of palm oil triacylglycerols are oleic (36–44%) and linoleic (9–12%) unsaturated fatty acids, which present *cis* configuration, and palmitic (39.3–47.5%) and stearic (3.5–6%) saturated fatty acids (Rincón and Martínez 2009). Furthermore, this oil contains high levels of vitamin A, an important nutrient not only for vision and protection against a number of serious health disorders, but also for proper immune function, growth, development, and gastrointestinal function. β -carotene besides presenting the highest vitamin A activity also has antioxidant capabilities and can function as a lipid radical scavenger and singlet oxygen quencher due to its unique structure of conjugated double bonds and

✉ Paula Andrea Osorio Carmona
osorio.carmona@gmail.com

¹ Embrapa Agroenergy, Parque Estação Biológica (pqEB), Av. W3 Norte (final), P.O. Box 40315, Brasília, DF 70770-901, Brazil

² Institute of Technology, Faculty of Mechanical Engineering, Federal University of Pará, Rua Augusto Corrêa, Guamá, P.O. Box 8619, Belém, PA 66075-900, Brazil

ionone rings (Donhowe et al. 2014). For these reasons, there is a strong interest in incorporating α - and β -carotene and other carotenoids as functional ingredients in food formulations (Donhowe and Kong 2014).

However, fatty acids and the poly-isoprenoid structure of carotenoid pigments, also responsible for their colorant properties and biological functions, are very sensitive to heat, moisture, light, and pro-oxidant conditions. Such factors provoke oxidation and isomerization reactions, which could decrease effectiveness as pigment as well as physiological benefits of carotenoids (Rascón et al. 2015).

Nowadays, eco-friendly and more efficient extraction techniques such as supercritical fluid CO₂ extraction are gaining importance. Supercritical CO₂ is a solvent widely used in the extraction process because of its mild critical temperature and pressure (304.2 K and 7.4 MPa) (Cardenas-Toro et al. 2014). Supercritical fluid extraction of PPF provides an oil rich in carotenoids, which can be microencapsulated for preservation and increase of their shelf life.

Among many methods, spray-drying is the most commonly used one due to its easiness of industrialization, continuous production, economical operation, high reproducibility, and possibility for handling labile materials because of the short contact time in the dryer (Aghbashlo et al. 2013). Both wall material selection and emulsion properties (total solids, stability, viscosity, and droplet size), besides controlling processing conditions during drying, can strongly affect parameters like efficiency, physical characteristics, product stability, and shelf life of final powder (Roccia et al. 2014).

Gum arabic (GA) is a highly branched heteropolymer of sugars, consisting of D-glucuronic acid, L-rhamnose, D-galactose, and L-arabinose, with approximately 2% protein covalently linked to the carbohydrate chain (Aniesrani Delfiya et al. 2015). GA has been the agent of choice for many years since it is nontoxic, odorless, and tasteless and provides film-forming ability, excellent emulsification capacity, low viscosity in aqueous solution, and satisfactory retention properties (Chranioti and Tzia 2014).

Accordingly, very little comprehensive information is available about the effect of operating conditions on microencapsulation by spray-drying of pressed palm fiber oil (PPFO). The aim of this study was to investigate the effect of solids content and to select the best operating conditions (drying air temperatures, feed flow rates, and atomization air flow rates) based on PPFO quality extracted with supercritical fluid and microencapsulated by spray-drying. For this purpose, microencapsulation efficiency (ME), peroxide value (PV), moisture content (MC), hygroscopicity, and microcapsules morphology produced at different drying conditions were analyzed as responses. Viscosity, stability, and droplet size of prepared emulsions were also measured experimentally to interpret the obtained results. Moreover, efficient microcapsules produced at optimal drying conditions, optimized using

Response Surface Methodology, were evaluated for major carotenoid identification and fatty acid profile. PPFO microparticles with favorable physicochemical properties can be considered as an additive with high potential for use as a natural coloring or in food fortification.

Materials and Methods

Chemicals and Materials

Solvents (analytical or spectrometric grade), sodium chloride, ammonium thiocyanate, barium chloride dehydrate, iron (II) sulfate heptahydrate, and iron reduced were purchased from Vetec (Rio de Janeiro, Brazil). Anhydrous sodium sulfate, butylated hydroxytoluene, *tert*-butyl methyl ether (MTBE), and carotenoid standards (HPLC grade) including β -carotene (C4582, type II synthetic, $\geq 95\%$), α -carotene (50887, $\geq 98\%$), and (9Z)- β -carotene (52824, $\geq 95\%$) were obtained from Sigma-Aldrich (Rio de Janeiro, Brazil). Methanol was acquired from Panreac (Alvorada, Brazil).

PPF was kindly donated by Denpasa (Pará, Brazil) and it is an industrial residue generated after palm oil extraction.

Gum arabic Instantgum BA® was kindly donated by Nexira (São Paulo, Brazil).

The PPFO supercritical extraction unit is an adaptation of the unit plant described by de França et al. (1999), which consists of a closed system composed by one extractor and two collectors, interconnected by valves in a recycle way. The solvent used was supercritical CO₂ (S.A. White Martins, 99.9% purity, Belém, Pará, Brazil), pressurized by a diaphragm-type compressor (model MKZ120-50, Andreas Hofer, Mülheim, Germany). PPF was previously dried in an oven (Quimis, Q314M242, Brazil) at 60 °C, during 4 h and the final moisture content was 7.01%. Then, approximately 1.0 kg of dry PPF was packed in a cylindrical wrap and arranged inside an extractor (10 cm diameter and 36 cm height). The extractor was heated to 60 °C with subsequent injection of CO₂ and pressurization up to 27 MPa. The collectors 1 and 2 were maintained at 15 and 6 MPa, respectively. Extraction time was 2.5 h and after finalization, the oils from collectors were mixed into a single extract, which was centrifuged to remove any solid particles.

Emulsions Preparation

Total solid content varied from 20 to 40% (w/w). GA dispersions were dissolved in distilled water, according to experimental design, under constant mechanical stirring (1000 rpm) at room temperature for 2 h and kept overnight at 4 °C to ensure full hydration of polymer molecules. Before emulsion preparation, all dispersions were heated up to 50 °C in a water bath. Carotenoid extract was also preheated at the same

temperature, and dropwise added into corresponding aqueous phase, at an active core/wall ratio of 1:4 w/w (Carneiro et al. 2013; Roccia et al. 2014, and Tonon et al. 2011), and blended using an UltraTurrax disperser (T25 D S32, IKA®-Labortechnik, Staufen, Germany) at 18,000 rpm for 5 min.

Emulsions Characterization

Creaming Index

Immediately after preparation, 10 ml of each emulsion was poured into a cylindrical glass tube (internal diameter = 15.5 mm, height = 65 mm), sealed with a plastic cap and stored at 25 °C. Emulsion stability was analyzed by the phase separation observed throughout 24 h after emulsion preparation.

Oil Droplet Size

The average oil droplet size of emulsions was determined by dynamic light scattering (DLS) technology using a Zeta PALS equipment (Brookhaven Instruments Corporation, Holtsville, USA). To avoid multiple scattering effects during measurement, emulsions were diluted to attain an oil-phase volume fraction of approximately 0.001% using Milli-Q water. Diluted emulsions were put into a folded capillary cell after stirring for 10 min. The droplet size and size distribution were measured at a fixed angle of 90° at 25 °C. The emulsion absorption value was adjusted to 0.001 and a relative refractive index $n_{oil}/n_{water} = 1.094$ ($n_{oil} = 1.45545$, $n_{water} = 1.33$) was used to data analyze, assuming that all droplets were spherical in shape (Nesterenko et al. 2014).

Emulsions Viscosity

The emulsions' apparent viscosities were determined with the aid of a rotational programmable rheometer (DV-III Ultra, Brookfield Engineering Laboratories, Stoughton, MA, USA) fitted with SC4-34 spindle. Samples were placed into a rheometer measurement cell, allowed to equilibrate for 5 min, and maintained constant at 25 °C by means of a thermostat tank (ThermoSel). Emulsion viscosity was measured by means of steady-shear flow curves (shear stress \times shear rate). Three flow ramps (up, down, and up-cycles) were obtained in a range of shear rates ranging from 1 to 70 s⁻¹ to eliminate any possible thixotropic effect. Rheograms obtained in the third ramp were fitted to empirical models and viscosity was calculated as the relationship between shear stress and shear rate. Apparent viscosity was obtained in terms of pascal-second (Pa.s).

Spray-Drying

The spray-drying process was performed in a laboratory-scale Mini Spray Dryer Büchi B-290 Advanced (Büchi Labortechnik AG, Flawil, Switzerland), with a main spray chamber of 65 \times 110 \times 70 cm and a two-fluid nozzle atomizer consisting of a 0.7-mm nozzle tip hole and a 1.5-mm nozzle cap. The air atomizing pressure was kept constant at 7 bars for all experiments and aspirator rate was set at 35 m³/h as recommended by the manufacturer.

A Rotatable Central Composite Design (RCCD) was used to assess the effect of independent variables on powder properties, considering four factors: feed total solid content (20–40%), feed volumetric flow rate expressed as percent of maximum peristaltic pump rate (8–32%), inlet air temperature (130–202 °C), and atomization air volumetric flow rate (20–60 mm). Five levels of each variable were chosen for the trials, including the central point and two axial points, totaling 28 experimental runs. Planning matrix is presented in Table 1 in real and codified variables.

Experimental data obtained was analyzed by the response surface method, using the following second-order polynomial equation (Eq. 1):

$$y = \beta_0 + \beta_1x_1 + \beta_2x_2 + \beta_3x_3 + \beta_4x_4 + \beta_{11}x_1^2 + \beta_{22}x_2^2 + \beta_{33}x_3^2 + \beta_{44}x_4^2 + \beta_{12}x_1x_2 + \beta_{13}x_1x_3 + \beta_{14}x_1x_4 + \beta_{23}x_2x_3 + \beta_{24}x_2x_4 + \beta_{34}x_3x_4 \quad (1)$$

where y is the response variable; β_n are constant regression coefficients, and x_1 , x_2 , x_3 , and x_4 are coded independent variables (solid content, feed flow rate, inlet air temperature, and atomization air flow, respectively).

Analysis of variance (ANOVA), test for lack of fit, regression coefficients determination, and three-dimensional graphs generation were carried out using the Statistica 12.0 software (StatSoft, Tulsa, USA). Considering that unsaturated fatty acids and carotenoids are chemically unstable in the presence of oxygen, light, moisture, and heat, the microencapsulation process optimization objective maximizing β -carotene and PPFO ME and minimizing lipid oxidation to preserve the bioactive properties and potential health beneficial effects of carotenoids and the PPFO chemical and sensorial quality.

Powder Analysis

Moisture Content

Particle moisture content was determined gravimetrically by drying in a forced-circulation oven at 105 °C until constant weight (Wang et al. 2011).

Table 1 Experimental design for PPFO microencapsulation by spray-drying

Tests	Solid content (%)	Feed flow rate (%)	Inlet air temperature (°C)	Atomization air flow (mm)
1	-1 (25)	-1 (14)	-1 (148)	-1 (30)
2	+1 (35)	-1 (14)	-1 (148)	-1 (30)
3	-1 (25)	+1 (26)	-1 (148)	-1 (30)
4	+1 (35)	+1 (26)	-1 (148)	-1 (30)
5	-1 (25)	-1 (14)	+1 (184)	-1 (30)
6	+1 (35)	-1 (14)	+1 (184)	-1 (30)
7	-1 (25)	+1 (26)	+1 (184)	-1 (30)
8	+1 (35)	+1 (26)	+1 (184)	-1 (30)
9	-1 (25)	-1 (14)	-1 (148)	+1 (50)
10	+1 (35)	-1 (14)	-1 (148)	+1 (50)
11	-1 (25)	+1 (26)	-1 (148)	+1 (50)
12	+1 (35)	+1 (26)	-1 (148)	+1 (50)
13	-1 (25)	-1 (14)	+1 (184)	+1 (50)
14	+1 (35)	-1 (14)	+1 (184)	+1 (50)
15	-1 (25)	+1 (26)	+1 (184)	+1 (50)
16	+1 (35)	+1 (26)	+1 (184)	+1 (50)
17	-2 (20)	0 (20)	0 (166)	0 (40)
18	+2 (40)	0 (20)	0 (166)	0 (40)
19	0 (30)	-2 (8)	0 (166)	0 (40)
20	0 (30)	+2 (32)	0 (166)	0 (40)
21	0 (30)	0 (20)	-2 (130)	0 (40)
22	0 (30)	0 (20)	+2 (202)	0 (40)
23	0 (30)	0 (20)	0 (166)	-2 (20)
24	0 (30)	0 (20)	0 (166)	+2 (60)
25	0 (30)	0 (20)	0 (166)	0 (40)
26	0 (30)	0 (20)	0 (166)	0 (40)
27	0 (30)	0 (20)	0 (166)	0 (40)
28	0 (30)	0 (20)	0 (166)	0 (40)

Hygroscopicity

Samples of about 1 g were evenly spread on aluminum capsules (70 mm diameter) and placed in desiccators with a NaCl saturated solution (75% RH), at 25 °C. After 1 week, samples were weighed and hygroscopicity was expressed as gram of absorbed moisture per 100 g of dry solids (g/100 g) (de Barros Fernandes et al. 2014).

Total and Non-encapsulated PPFO in Microparticles

Total PPFO content was assumed to be equal to the initial core material, since preliminary tests revealed that all the initial oil was retained in the powder ($p > 0.05$, data not shown), which was expected, since PPFO is not volatile. Surface PPFO was determined according to Bae and Lee (2008). PPFO microencapsulation efficiency was calculated from Eq. 2:

$$ME_{PPFO}(\%) = \left[\frac{\text{Total PPFO} - \text{Surface PPFO}}{\text{Total PPFO}} \right] \times 100. \quad (2)$$

β -Carotene Content from Emulsions

β -carotene content in infeed emulsions was determined according to the method described by Deng et al. (2014), with some modifications. Emulsion samples (0.5 g) were subjected to solvent extraction by adding acetone (2 mL) and the mixture was vortexed for 5 s. After adding 2 mL of petroleum ether and deionized water (10 mL), the tubes were placed in a sonicating water bath for 1 min and the organic layer (upper layer) was transferred to a test tube with aid of a Pasteur pipette. This process was repeated until the bottom aqueous phase was clear and colorless. Ethereal phases were pooled and dehydrated using anhydrous Na_2SO_4 . Adsorption of the resultant organic was spectrophotometrically measured at a wavelength of 450 nm on a Cary 60 UV–Vis spectrophotometer (Agilent Technologies, Santa Clara, USA). β -carotene content was calculated considering the absorption coefficient of β -carotene in petroleum ether $A_{1\text{cm}}^{1\%} = 2592$, according to Rodriguez-Amaya and Kimura (2004):

Emulsion β -carotene(g/g of oil)

$$= [A_{450\text{nm}} \times y(\text{mL}) \times 10^4] / (A_{1\text{cm}}^{1\%} \times W_{\text{oil}}) \quad (3)$$

where $A_{450\text{nm}}$ represents the oil absorbance, $y(\text{mL})$ is the total volume of extract, and W_{oil} represents the oil weight in analyzed sample.

Total and Surface β -Carotene and Microencapsulation Efficiency

Surface β -carotene content was performed according to Deng et al. (2014). Fifty milligrams of each powder was extracted with 25 mL of petroleum ether. After shaking at 100 rpm for 15 s, the dispersion was centrifuged at $1000 \times g$ for 1 min. The adsorption of the resultant supernatant was determined at 450 nm. For analysis of the β -carotene content in encapsulated powders, about 100 mg of powder was weighted into 30 mL glass tubes, reconstituted in 1 mL of distilled water, and vortexed for 3 min. The reconstituted samples were subjected to solvent extraction by adding acetone (2 mL) and the mixture was vortexed for 5 s. The other steps and total β -carotene calculation were performed exactly as described for determining the β -carotene content from emulsions (“ [\$\beta\$ -carotene content from emulsions](#)” section).

β -carotene ME was calculated as the β -carotene percentage in microparticle core in relation to its concentration in feed emulsion as follows:

$$\text{ME}_{\beta\text{-carotene}}(\%) = [(\beta\text{-car}_{\text{total in PPFO}} - \beta\text{-car}_{\text{superficial in PPFO}}) / \beta\text{-car}_{\text{in feed emulsion}}] \times 100 \quad (4)$$

Peroxide Value

PV determination was carried out according to Szterk et al. (2013). Reconstituted emulsions after drying (100 μL) were obtained by dispersing 0.1 g of powders in 0.35 mL deionized water. That water volume was used to rehydrate microcapsules to similar conditions of entry into the spray dryer according to the total solids contents (dry matter) of emulsion. Mixing was done with vortex for 6 min at room temperature ($\sim 20^\circ\text{C}$). The other steps were performed as described by the aforementioned authors. Absorbance was measured at 480 nm and hydroperoxide concentrations were determined using a Fe^{+3} standard curve (Hornero-Méndez et al. 2001) and expressed as milliequivalents peroxide per kilogram of oil.

PPFO Fatty Acid Determination by Gas Chromatography

PPFO fatty acid composition was determined by fatty acid methyl ester (FAME) gas chromatography, according to

official AOCS methods Ce 2-66 and Ce 1-62 (AOCS 1989). Chromatographic analysis was performed with an Agilent 7890A gas chromatograph (Palo Alto, USA), equipped with a split-splitless injector, a flame ionization detector (FID), and a HP-88 capillary column (60 m \times 0.25 mm i.d. and 0.2 μm film thickness, Agilent Tech.). One microliter of sample was injected into the column. The injection was performed in split mode with a split ratio of 50:1. Oven temperature was 140°C for 5 min and then programmed to ramp from 140 to 240°C at $4^\circ\text{C}/\text{min}$, held at 240°C for 5 min. Injector and detector temperatures were set at 260°C . Helium was used as carrier gas at a constant flow rate of 1 mL/min. Nitrogen gas was used as make up gas (25 mL/min); flow of hydrogen gas and synthetic air were provided at 30 and at 400 mL/min, respectively. FAME was identified by comparison of relative retention times of FAME peaks from samples with the standard mixture Supelco 37 Component FAME Mix (Cat. No. 47885-U).

High-Performance Liquid Chromatography Analysis of Carotenes

Carotenoids from pure PPFO (10 mg) or encapsulated PPFO (100 mg) were extracted and transferred to petroleum ether as previously described for the quantification of total β -carotene content in encapsulated powder. After partition to petroleum ether, the carotenoid solution was saponified with an equal volume of 10% KOH in methanol overnight at room temperature, with nitrogen flush into a blending vessel (Rodríguez-Amaya and Kimura 2004). The saponified sample was then extracted with 50-mL portions of petroleum ether until extracts became colorless. The combined petroleum ether extracts were washed five times with 50-mL portions of distilled water to remove the alkali, and carotenoid phases was collected and dried with anhydrous Na_2SO_4 . A portion of extract was brought to dryness under a nitrogen stream. The residue was dissolved in a known volume of a mixture methanol/MTBE 50:50 (v/v) and filtered through a 0.22- μm filter, 10 μL of which was injected into HPLC.

The LC system used was an Agilent's 1290 Infinity HPLC system equipped with a Thermostat (G1330B), DAD (G4212A), binary pump (G4220A), TCC (G1316C), and autosampler (G4226A). Analytical separations were carried out on a stainless steel (250 \times 4.6 mm i.d.) Develosil UG C₃₀ (5 μm particle size) column (Nomura Chemical, Sojo, Japan). Elution was performed following a linear mobile phase gradient using solvent A (81:15:4 methanol/MTBE/water) and solvent B (46:50:4 methanol/MTBE/water), 0 min (50:50), 45 min (5:95), 45.01 min (50:50), and 55 min (50:50) at a flow rate of 1 ml/min. The column was thermostated at 16°C and the detection wavelength was adjusted to 450 nm. Commercial standards and spectral data were used to assign carotenoid peaks. All *E*- and *Z*- β -carotene isomer and α -carotene were quantified by means of

Table 2 Droplet mean diameter, viscosity, and stability of emulsions produced with different solid concentrations

Solid content (%)	Droplet mean diameter (μm)	Viscosity (Pa·s)	24-h emulsion stability (phase separation)
20	1.58 ± 0.23^a	0.03 ± 0.00^e	No
25	1.22 ± 0.14^b	0.06 ± 0.01^d	No
30	1.09 ± 0.17^{bc}	0.14 ± 0.00^c	No
35	1.03 ± 0.09^c	0.34 ± 0.00^b	No
40	0.99 ± 0.02^c	0.69 ± 0.01^a	No

Mean values in the same column with different letters are significantly different (Tukey, $p \leq 0.05$)

calibration curves. Results were expressed in microgram of carotenoids per gram of oil.

Scanning Electron Microscopy

The powders morphological properties were observed in a scanning electron microscope Carl Zeiss Sigma HV using a Gemini column and in-lens secondary electron detector. Samples were pulverized over a carbon tape fixed directly on the sample holder stubs of 12 mm in diameter and then subjected to metallization (sputtering) with a 10-nm thin layer of gold in an equipment Quorum Q150T ES. After metallization, samples were observed with magnifications of $\times 4000$, $\times 5000$, and $\times 10,000$ (Ferreira et al. 2016).

Results and Discussion

Emulsions Characterization

Stability and Emulsion Viscosity

Emulsions were observed during 24 h after blending. According to Table 2, regardless of total solids concentration, all emulsions were kinetically stable, without phase

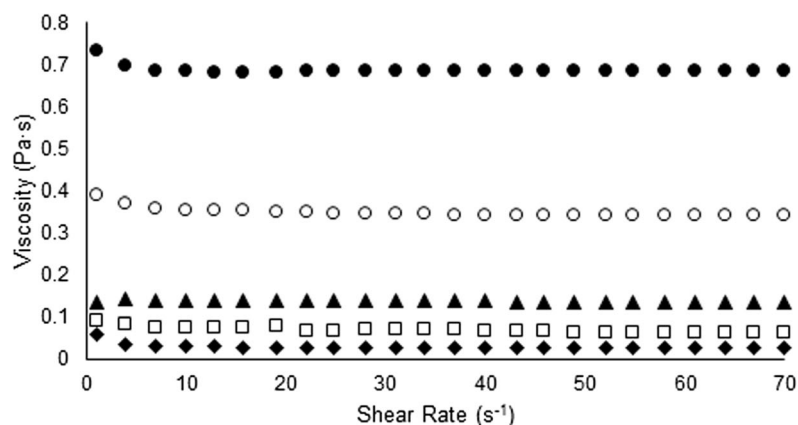
separation. Kinetically stable emulsions during the oils' microencapsulation by spray-drying are known to be determinant in retention and shelf life of encapsulated hydrophobic molecules by reduction of surface oil content on particles (Bustamante et al. 2016).

As stated before, emulsion viscosity was determined through steady-shear flow curves. The apparent viscosity of emulsions produced with different solid contents of GA is shown in Fig. 1.

Experimental data were adequately adjusted by the Newtonian model, according to which apparent viscosity is constant with increasing shear rate. The upward and downward curves of all tests were superimposed, verifying absence of hysteresis effect between the outward (increasing) and returning (down) curves. These results indicate that fluids present time-independent rheological behavior and did not show thixotropy. Roccia et al. (2014) also observed a Newtonian behavior in emulsions produced with sunflower oil and blends of maltodextrin and hydroxypropylmethylcellulose as wall materials.

Emulsion viscosity increased as total solid content increased (Table 2), which was expected, since GA has a ramified structure with long chains and is generally used as a thickening agent in foodstuffs, making them more viscous (Aniesrani Delfiya et al. 2015). According to Zaeim et al.

Fig. 1 Emulsions viscosity prepared with different solids content as a function of shear rate



◆ 20% Total Solids □ 25% Total Solids ▲ 30% Total Solids ○ 35% Total Solids ● 40% Total Solids

(2018), GA shows a Newtonian flow behavior at shear rates higher than 10 s^{-1} and concentrations between 20 and 40% (w/w).

Oil Droplet Size

The droplets mean diameter of emulsions prepared with different solid contents is presented in Table 2. Droplet diameter range from 0.99 to $1.58 \mu\text{m}$ and the decrease in total solid content resulted in the biggest droplets size. Castel et al. (2017) pointed out that at low solid contents, molecules available would not be enough to completely cover the oil-water interface created during the emulsification process, favoring coalescence and resulting in formation of larger droplets. On the other hand, as observed in Table 2, emulsions produced with the highest solid content (40%) was the most viscous (0.69 Pa·s) and showed the lowest droplet mean diameter

($0.99 \mu\text{m}$). Highly viscous emulsions imply in a greater resistance to droplets movement, avoiding aggregation, and resulting in smaller diameters.

Response Surface Analysis

The MC, hygroscopicity, β -carotene, and PPFO ME and PV values for each trial of experimental design are presented in Table 3.

Table 4 shows the regression coefficients for coded second-order polynomial equations, calculated and tabulated F values, and determination coefficients (R^2). Non-significant terms were eliminated and the resulting equations were tested for adequacy and fitness of developed models by ANOVA. The fitted models were suitable, showing significant regression and satisfactory determination coefficients. These facts, together with the low residual values and the non-significant

Table 3 Moisture content, hygroscopicity, β -carotene and PPFO ME, and peroxide value for the 28 trials of the experimental design

Tests	MC (%)	Hygroscopicity (g water/100 g d.b.)	β -carotene ME (%)	PPFO ME (%)	PV (meq/kg oil)
1	2.24 ± 0.27	16.25 ± 0.31	67.01 ± 0.72	80.29 ± 0.82	2.84 ± 0.08
2	2.46 ± 0.05	16.19 ± 0.20	70.95 ± 1.27	80.84 ± 0.09	2.56 ± 0.01
3	2.94 ± 0.18	15.85 ± 0.15	73.75 ± 1.14	74.93 ± 0.40	3.99 ± 0.14
4	2.16 ± 0.08	16.19 ± 0.11	75.75 ± 2.39	79.18 ± 2.48	3.68 ± 0.03
5	1.03 ± 0.01	17.37 ± 0.12	75.42 ± 1.13	79.59 ± 0.23	3.87 ± 0.02
6	0.76 ± 0.01	18.33 ± 0.12	77.24 ± 1.76	76.49 ± 0.06	3.49 ± 0.09
7	0.92 ± 0.06	17.01 ± 0.16	78.39 ± 2.61	83.26 ± 1.39	5.07 ± 0.10
8	0.80 ± 0.01	18.12 ± 0.23	78.65 ± 0.94	78.01 ± 0.54	4.85 ± 0.09
9	2.78 ± 0.02	15.89 ± 0.09	61.69 ± 1.72	68.52 ± 1.56	4.54 ± 0.20
10	2.67 ± 0.12	15.95 ± 1.46	78.59 ± 1.81	90.85 ± 0.01	2.10 ± 0.17
11	3.87 ± 0.13	15.41 ± 0.09	62.98 ± 1.24	65.14 ± 0.96	4.85 ± 0.10
12	2.75 ± 0.16	15.64 ± 0.09	81.38 ± 3.86	91.32 ± 0.20	2.06 ± 0.72
13	1.59 ± 0.05	16.83 ± 0.92	66.27 ± 0.75	72.73 ± 1.19	5.70 ± 0.18
14	1.63 ± 0.07	16.79 ± 0.2	79.54 ± 4.08	83.50 ± 1.74	2.28 ± 0.21
15	1.32 ± 0.17	16.39 ± 0.29	67.58 ± 0.26	68.21 ± 0.94	7.42 ± 0.60
16	1.66 ± 0.02	17.24 ± 0.10	84.32 ± 1.35	85.36 ± 0.76	2.32 ± 0.09
17	2.28 ± 0.08	16.65 ± 0.22	61.37 ± 0.58	72.84 ± 1.44	4.76 ± 0.18
18	1.70 ± 0.15	16.93 ± 0.29	85.61 ± 1.19	84.22 ± 0.23	1.76 ± 0.07
19	1.00 ± 0.02	17.52 ± 0.85	63.31 ± 6.11	78.47 ± 0.14	4.12 ± 0.53
20	3.25 ± 0.19	16.14 ± 0.79	67.84 ± 0.57	71.01 ± 1.22	4.72 ± 0.48
21	2.61 ± 0.04	15.05 ± 0.21	63.64 ± 1.93	68.64 ± 0.73	5.15 ± 0.15
22	0.42 ± 0.05	16.97 ± 0.11	65.70 ± 1.18	73.47 ± 0.34	6.18 ± 0.60
23	2.45 ± 0.05	17.18 ± 0.26	72.66 ± 0.54	74.57 ± 0.36	2.19 ± 0.27
24	1.51 ± 0.04	16.97 ± 0.68	69.98 ± 2.39	75.13 ± 1.12	4.79 ± 0.15
25	2.50 ± 0.06	16.37 ± 0.27	70.54 ± 1.75	75.68 ± 1.93	2.80 ± 0.46
26	1.39 ± 0.12	17.47 ± 0.08	71.71 ± 1.10	81.37 ± 0.81	3.16 ± 0.01
27	2.14 ± 0.29	16.62 ± 0.07	71.82 ± 1.17	76.80 ± 1.67	3.19 ± 0.21
28	1.59 ± 0.31	17.45 ± 0.32	69.50 ± 0.85	76.59 ± 4.14	3.25 ± 1.45

MC moisture content, ME microencapsulation efficiency, PPFO pressed palm fiber oil, PV peroxide value

Table 4 Coded second-order regression coefficients for moisture content, hygroscopicity, β -carotene and PPFO ME, and peroxide value

Regression coefficient	MC (%)	Hygroscopicity (g water/100 g)	β -carotene ME (%)	PPFO ME (%)	PV (meq /kg oil)
β_0	1.944	16.875	70.592	77.394	3.123
β_1	N.S.	0.168	5.075	3.985	-0.872
β_{11}	N.S.	N.S.	1.525	N.S.	N.S.
β_2	0.239	-0.188	1.465	N.S.	0.337
β_{22}	N.S.	N.S.	N.S.	N.S.	0.267
β_3	-0.690	0.607	1.643	N.S.	0.436
β_{33}	N.S.	-0.239	N.S.	N.S.	0.577
β_4	N.S.	-0.232	N.S.	N.S.	0.253
β_{44}	N.S.	N.S.	N.S.	N.S.	N.S.
β_{12}	N.S.	N.S.	N.S.	N.S.	N.S.
β_{13}	N.S.	N.S.	N.S.	-2.109	N.S.
β_{14}	N.S.	N.S.	3.581	4.998	-0.785
β_{23}	N.S.	N.S.	N.S.	N.S.	N.S.
β_{24}	N.S.	N.S.	N.S.	N.S.	N.S.
β_{34}	N.S.	N.S.	N.S.	N.S.	N.S.
R^2	0.672	0.802	0.796	0.764	0.876
$F_{\text{calculated}}$	25.694	17.854	17.160	25.924	20.215
$F_{\text{tabulated}}$	3.385	2.661	2.661	3.009	2.514
Regression (p value)	$p < 0.001$	$p < 0.001$	$p < 0.001$	$p < 0.001$	$p < 0.001$

β_n are constant regression coefficients and x_1 , x_2 , x_3 , and x_4 are coded independent variables (solid content, feed flow rate, inlet air temperature, and atomization air flow, respectively)

MC moisture content, ME microencapsulation efficiency, PPFO pressed palm fiber oil, PV peroxide value

lack of fit of models ($p > 0.01$) show that quadratic polynomial equations are adequate for predicting actual relationships between dependent and independent variables.

Moisture Content

According to Table 3, the MC of powders varied from 0.42 to 3.87% and was affected by pump setting and the inlet air temperature (Table 4). High feed flow rate produced powders with the highest MC, while high drying temperatures decreased the MC of particles. Increasing the inlet air temperature provides more energy for water evaporation from droplet/particle because of the higher heat and mass transfer rates (Aghbashlo et al. 2013). The reduction of powder moisture content with increasing inlet air temperature was also observed in spray-dried coffee oil (Frascareli et al. 2012). On the other hand, the increase in feed flow rate led to an increase on particle moisture content. This can be attributed to the shorter contact time between feed and drying air, making the heat transfer less efficient and resulting in lower water evaporation. The effect observed of pump rate on moisture content is particularly in agreement with results reported by Gallo et al. (2011) for spray-drying of *Rhamnus purshiana* using colloidal silicon dioxide as a carrier agent.

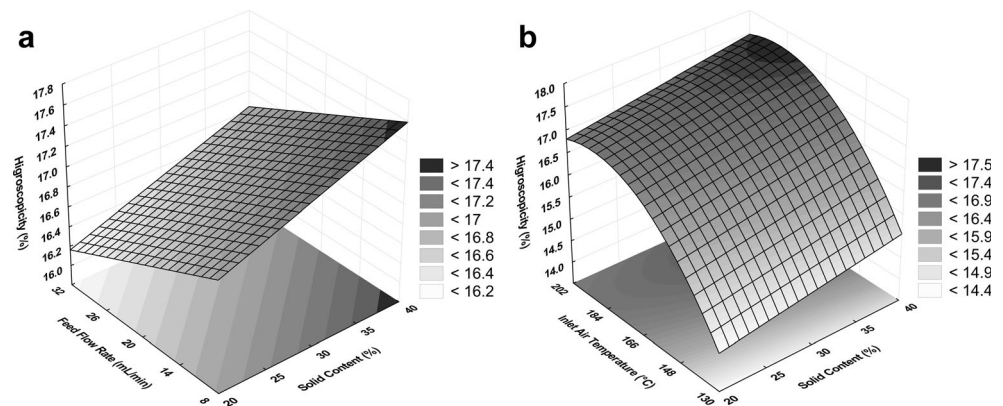
Hygroscopicity

Figure 2 shows the response surface for hygroscopicity as a function of total solid content, feed flow rate, and inlet air temperature.

Higher GA concentrations resulted in more hygroscopic microparticles (Fig. 2). This could be attributed to the hygroscopic nature of GA and to the increased viscosity in emulsions with high solid concentrations, which implies less water available for evaporation, resulting in powders with lower MC and, consequently, more hygroscopic. Similar results were observed by Silva et al. (2013) in encapsulation of jaborcaba peel extracts by spray-drying, where the substitution of 30% maltodextrin by a mixture of 25% GA with 5% maltodextrin resulted in highly hygroscopic powders.

Inlet air temperature and feed flow rate also influenced particles' hygroscopicity (Table 4). The highest hygroscopicity values were obtained with increasing temperatures and decreasing flow rates (Fig. 2), which were the variables that affected powders' MC, in an opposite way. This indicates that the lower the particles' MC, the higher their hygroscopicity, i.e., the greater their capacity to adsorb ambient moisture, which is related to the greater water concentration gradient between the product and the surrounding air (Tonon et al. 2008). These results are in agreement with those published

Fig. 2 Response surface for hygroscopicity of PPFO particles produced **a** at a temperature of 166 °C and atomization air flow of 40 mm and **b** at a feed flow rate of 20 ml/min and atomization air flow of 40 mm



by Castro-Muñoz et al. (2015), in their work about spray-drying of purple cactus pear. Varying the gelatin/maltodextrin ratio and the drying inlet air temperature, the authors verified that powders' hygroscopicity conversely increased with particles' moisture content.

Microencapsulation Efficiency of β -Carotene

According to Tables 3 and 4, β -carotene ME varied from 61.37 to 85.61% and was significantly influenced by solid content, feed flow rate, and inlet air temperature. Figure 3 shows the response surfaces obtained for this response.

Total solid was the factor that most affected β -carotene ME (Table 4), and the higher the solids concentration, the higher the amount of encapsulated β -carotene was. As stated before, higher solids content resulted in higher emulsion viscosity, which implies shorter time to form a semi-permeable membrane around the atomized droplet, making the oil diffusion to the drying particle surface difficult (Roccia et al. 2014). In addition, the droplet size decreased when emulsion viscosity increased. According to Rajabi et al. (2015), the increase in emulsion viscosity could act effectively in protecting bioactive ingredients against thermal degradation and other destructive agents during the drying stage by increasing the surface-to-volume ratio due to decrease in size of atomized droplets. Frascareli et al. (2012), studying the microencapsulation of coffee oil using gum Arabic as wall material, also verified that the encapsulation efficiency was influenced by total solids content. The authors attributed these results to the emulsion properties, such as viscosity and droplet size.

The feed flow rate showed a positive effect on β -carotene ME, that is, the increase on this parameter resulted in greater microencapsulation efficiencies, which is probably related to the slower heat and mass transfer and to the lower energy supply occurring when the process was carried out with higher feed flow, resulting in lower β -carotene degradation. However, according to Fig. 3d, powders produced with feed flow rates greater than 26% should be dried at a minimum of 184 °C to achieve high β -carotene ME.

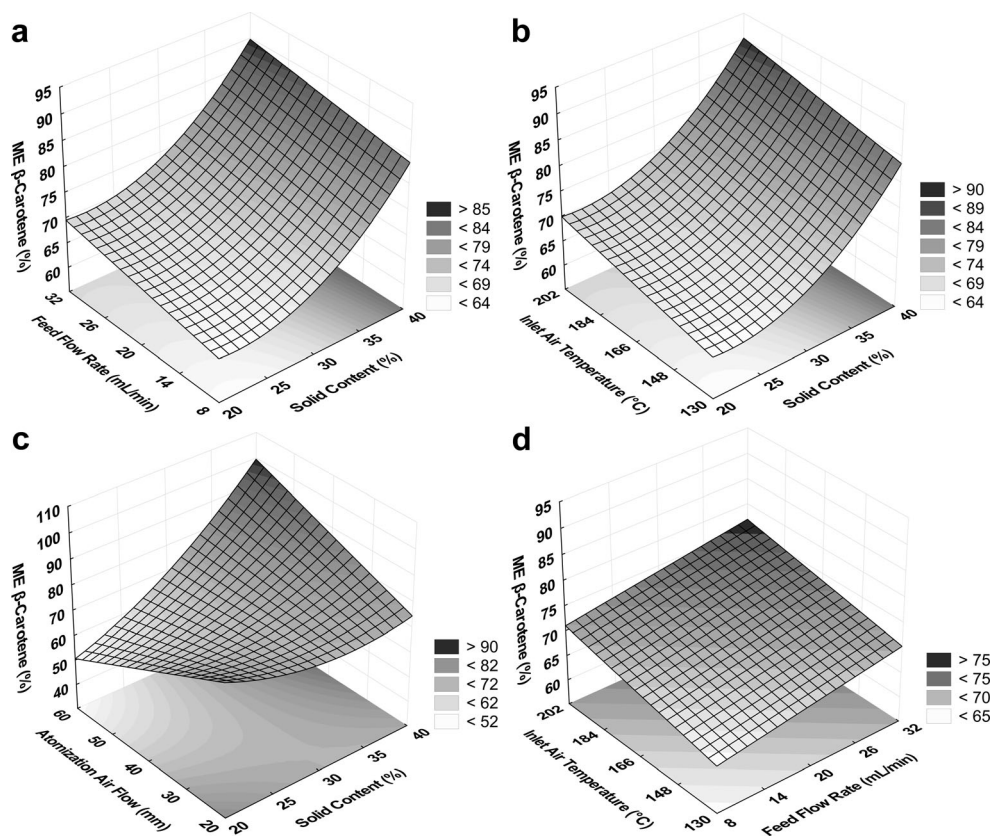
With respect to inlet air temperature, higher drying temperatures resulted in higher β -carotene ME (Table 4). According to Figs. 3b, d, the β -carotene ME increased with increasing temperature from 130 to 184 °C. However, a further increase up to 202 °C reduced the β -carotene ME (65.70%), which could be related to oxidation and/or degradation reactions induced by heat. Aniesrani Delfiya et al. (2015) also verified higher encapsulation efficiencies increasing the inlet air temperature from 150 to 175 °C in spray-drying of turmeric oleoresin. On the other hand, lower encapsulation efficiencies were obtained for powders produced at 200 °C. Bustamante et al. (2016), working with microencapsulation of *Haematococcus pluvialis* oleoresins, also observed that high inlet air temperatures during the spray-drying process produced losses of astaxanthin. The authors pointed out that particles produced at an inlet air temperature of 161 °C would maximize the astaxanthin ME. According to Kha et al. (2014), at higher drying temperatures, the excessive evaporation results in membranes with cracks, which can induce premature release and allow permeability to gases, compromising the retention and protection of encapsulated ingredient due to the susceptibility to degradation reactions. Therefore, it is important to determine the appropriate drying temperature to avoid such damage to the product.

Microencapsulation Efficiency of PPFO

PPFO ME varied from 65.14 to 91.32% (Table 3) and was significantly influenced by solid content and by interactions solid content \times inlet air temperature and solid content \times atomization air flow (Table 4).

Higher PPFO ME was observed when higher total solids content were used. Analogous to the β -carotene ME, these results can be attributed to emulsion properties. The higher the feed solid content, the higher was the emulsion viscosity. Emulsions with higher viscosity imply a smaller volume of water to be evaporated and require shorter time to form a crust, thus reducing circulation movements inside the droplets and resulting in higher active material retention. In addition,

Fig. 3 Response surface for β -carotene ME of particles produced **a** at a temperature of 166 °C and atomization air flow of 40 mm, **b** at a feed flow rate of 20 ml/min and atomization air flow of 40 mm, **c** at a feed flow rate of 20 ml/min and at a temperature of 166 °C, and **d** with solid of 30% and atomization air flow of 40 mm



emulsions produced with higher solids content showed lower droplet mean diameters, which resulted in higher ME, as stated before.

Positive effect of interaction solid content \times atomization air flow ratio (Table 4) indicated that the increase in solid content combined with high atomization air flow resulted in higher PPFO ME. According to Aghbashlo et al. (2013), the increase of encapsulation efficiency related to higher air flow rate can be attributed to the faster crust formation, which does not allow the oil to diffuse out to the particle surface.

However, higher solid contents associated with higher inlet air temperatures resulted in particles with lower PPFO ME as evidenced by the negative effect of interaction between these variables (Table 4). Similarly to the β -carotene ME, high drying temperatures (above 184 °C) resulted in lower amounts of PPFO trapped within solid particles. According to Balasubramani et al. (2015), high inlet air temperature can break the balance between the rate of water evaporation and film formation, which will lead to microcapsules breakdown and thus to lower oil retention. Jafari et al. (2008) suggested that a high enough inlet air temperature could (160–220 °C) cause heat damage to dry product, or “ballooning” and excessive bubble growth and surface imperfections, which increase losses during spray-drying. The lower the oil ME, the higher the amount of surface oil, which affects powders’ wettability

and dispersibility and increases susceptibility to oxidation and development of off-flavors, thus compromising the product acceptability (Balasubramani et al. 2015).

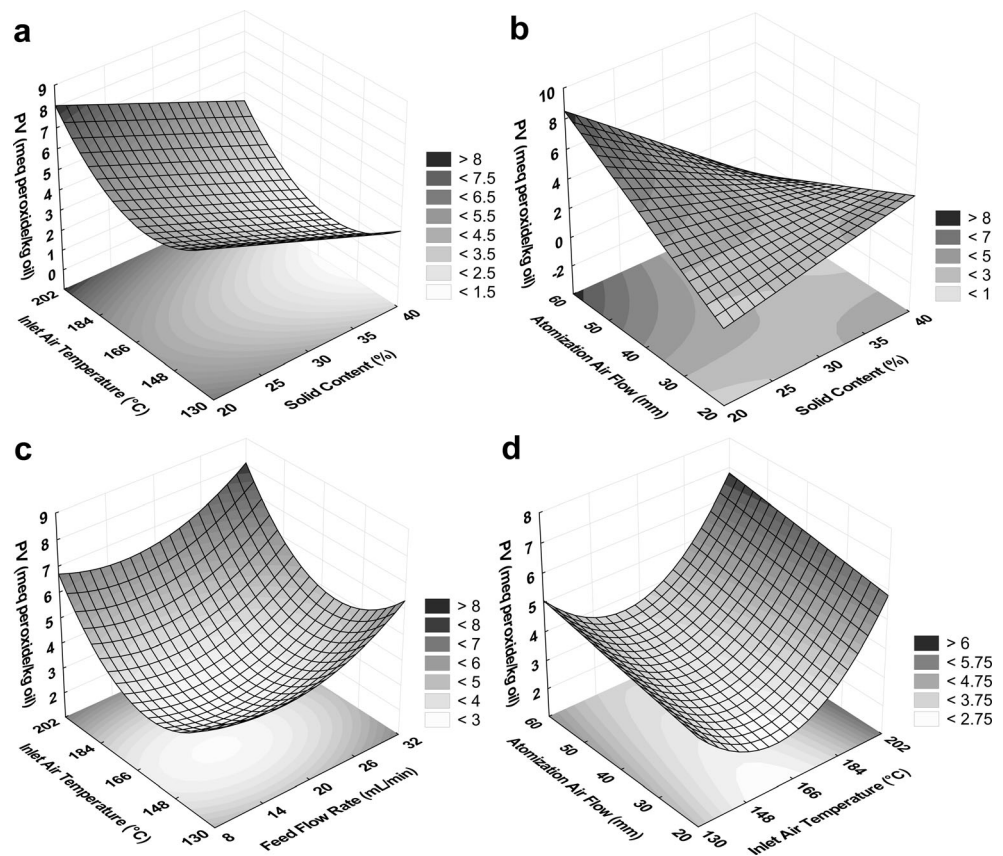
Peroxide Value

The influence of solid content, feed flow rate, inlet air temperature, and atomization air flow on peroxide value is shown in Fig. 4.

PV varied from 1.76 to 7.42 meq peroxide/kg oil (Table 3) and was affected by all independent variables (Table 4).

In general, higher solid content and lower atomization air flows led to lower PV. Moreover, negative effect of interaction solid content \times atomization air flow indicated that the increase in solid content combined with atomization air flow up to values around 40 mm resulted in particles with lower PV (Fig. 4b). This can be related to the higher PPFO ME obtained at these conditions, which led to an increase of oil protection against oxidation. The higher the PPFO ME, the lower the amount of oil on particle surface, which when in contact with oxygen, is much more susceptible to lipid oxidation than the encapsulated one. Aghbashlo et al. (2013) also verified that the increase in spraying air flow rate increased the fish oil encapsulation efficiency and decreased the lipid oxidation,

Fig. 4 Response surfaces for peroxide value of particles produced **a** at a feed flow rate of 20 mL/min and atomization air flow of 40 mm, **b** at a feed flow rate of 20 mL/min and at a temperature of 166 °C, **c** with solid of 40% and atomization air flow of 40 mm, and **d** with solid of 30% and a feed flow rate of 20 mL/min



due to the lower amount of superficial oil exposed directly to oxygen contact.

According to Fig. 4c, the increase in feed flow rate led to an increase in PV, which can be attributed to the greater particle moisture content observed when the feed flow rate increased above 26%, resulting in inefficient drying (response surface not shown). High moisture content can induce stickiness of powder particles, resulting in formation of inter-particle bridges that lead to caking and particle collapse, releasing the core material and favoring the lipid oxidation (Wang et al. 2011).

PV also increased with increasing drying temperatures. According to Fig. 4a, lipid oxidation was minimized at solid contents varying between 35 and 40% and inlet air temperatures in the range of 148 and 184 °C. Optimum values obtained for solids content can be attributed to emulsions properties, since the increase in solids content led to an increase in emulsions viscosity, reducing the droplets' internal circulation and mean diameter, which resulted in higher ME. Inlet air temperatures lower than 148 °C may not be sufficient for droplet drying, leading to an inefficient encapsulation, while temperatures higher than 184 °C accelerate the lipid oxidation reaction. According to Tonon et al. (2011), the use of higher inlet air temperatures provides more energy available for the lipid oxidation process, which occurs more intensely, favoring peroxides formation. Kha et al. (2014) similarly verified strong dependence of lipid oxidation on temperature. These authors

observed that PV of microencapsulated gac oil was almost twice higher for powders produced at inlet/outlet temperatures of 162/80 °C, when compared to that produced at 148/80 °C.

According to Ixtaina et al. (2015), oxidation products developed during spray-drying are in the initial stage and might be still in the form of oxidation precursors or free radicals only, since the particle exposure to heat is in the range of a few seconds at the most. When the drying process has finished, the product is in a solid state and the oxidation reaction rate is slow.

Process Optimization for PPFO Microencapsulation and Model Verification

The experimental design showed that all fitted models were suitable to describe the experimental data. However, the optimization was applied to maximizing β -carotene and PPFO ME and minimizing lipid oxidation.

In general, higher solid contents led to the increase of β -carotene and PPFO ME and decrease of PV, which were related to the emulsion droplet size and viscosity. However, feed emulsion prepared with the highest solids concentration (40%) led to adhesion of powders to the drying chamber wall, resulting in decreasing powder yield (data not shown). Therefore, optimum solid content was defined as 35%.

Although lower feed flow rates resulted in microcapsules with lower moisture contents and PV, the increase of this variable led to higher β -carotene ME. Therefore, to preserve the bioactive compounds functional properties of interest, the peristaltic pump rate was set at 26%, thus reducing the contact time between the emulsion and the drying air.

Considering that carotenoids and unsaturated fatty acids are chemically unstable in adverse conditions like heat, 166 °C was selected as the suitable temperature level for PPFO encapsulation to preserve the oil chemical and sensorial quality and to prevent the carotenoids' degradation. This temperature also provided oxidative stability to encapsulated PPFO.

Since the PV increased when higher atomization air flow was used and considering that this variable had significant negative effect on process yield (data not shown), one of the major factors for microencapsulation, the atomization air flow, was fixed at 40 mm.

Therefore, the selected optimal conditions were 35% of total solids, feed flow rate of 26%, inlet air temperature of 166 °C, and atomization air flow of 40 mm.

Utilizing these conditions, predicted values for hygroscopicity, β -carotene ME, PPFO ME, and PV of 16.86 g water/100 g, 78.66%, 81.38%, and 2.85 meq/kg oil, respectively, were obtained (Table 5). The experimental values for all response variables studied were consistent with the predicted ones, showing relative error values inferior to 8.0%. Thus, the quadratic models obtained by RCCD to describe these responses could be considered predictives.

Fatty Acid Composition of Pure and Encapsulated PPFO

The most abundant fatty acids in PPFO corresponded to monounsaturated (50.30%), followed by saturated (39.00%) and polyunsaturated (10.66%) acids, with oleic acid (49.04%), palmitic acid (23.85%), and linoleic acid (10.21%) being the most representative of each group, respectively (Table 6).

Unsaturated fatty acids accounted for 60.96% of total fatty acid content, which could contribute to the reduction of serum total cholesterol formation. The *sn*-2 position of palm oil triacylglycerols is mainly esterified with oleic and linoleic acid. This provides improved bioavailability of oleic acid as

monounsaturated fatty acid and linoleic acid as an essential fatty acid, as compared to oils or fats with similar composition but with randomized fatty acid distribution (Gee 2007). The bioavailability importance of oleic and linoleic unsaturated fatty acids is due to its hypocholesterolemic effect, decreasing LDL concentrations and potentiating beneficial actions of HDL cholesterol (Rincón and Martínez 2009).

In general, few differences were observed among pure and encapsulated PPFO. Both monounsaturated (oleic) and polyunsaturated (linoleic and linolenic) fatty acids, as well as saturated fatty acids (palmitic), showed a small but statistically significant decrease ($p < 0.05$) after microencapsulation (Table 6). However, the percentages of saturated fatty acids (SFAs) and monounsaturated fatty acids (MUFAs) losses (1.16 and 1.07%, respectively) were equivalent and significantly lower than the ones observed for polyunsaturated fatty acids (PUFAs) (1.82%). Therefore, PUFAs were more instable during the drying process. Generally, the greater the number of double bonds in fatty acids, the greater the susceptibility to oxidative deterioration, a degradative pathway that is affected by oxygen, light, temperature, and humidity (Ferreira et al. 2016).

The little change verified in fatty acid profile in pure and encapsulated PPFO can be related to the presence of carotenoids, which are antioxidants of great importance in stability, since they act by inhibiting or slowing down processes of lipid peroxidation on unsaturated fatty acids, which involves hydrolysis of ester bond in triglycerides and release of fatty acids that generate peroxides and hydroperoxides, responsible for changes in oil organoleptic characteristics (Rincón and Martínez 2009).

Major Carotenoids Identification of Pure and Encapsulated PPFO

According to Table 7, the PPF extraction with supercritical CO₂ allowed obtaining an extract with high concentrations of total carotenoids (2910.55 μ g/g oil). Furthermore, the average carotenoid content of encapsulated PPFO was statistically equivalent (2775.79 μ g/g oil), which allows to infer that microencapsulation is an interesting process for carotenoid preservation, since the PPFO remained an important source of bioactive compounds even after drying.

Table 5 Experimental (Exp.) and predicted (Pred.) values of powders produced at the optimal condition (35% solids, 26% feed flow rate, 166 °C inlet air temperature, and 40 mm atomization air flow)

	Hygroscopicity (g water/100 g)	β -carotene ME (%)	PPFO ME (%)	PV (meq/kg oil)
Exp.	18.15 \pm 0.20	80.00 \pm 1.67	81.24 \pm 0.59	2.99 \pm 0.37
Pred.	16.86	78.66	81.38	2.85
RE (%)	7.13	1.68	0.17	4.42

RE relative error, ME microencapsulation efficiency, PPFO pressed palm fiber oil, PV peroxide value

Table 6 Fatty acid composition of pure and encapsulated PPFO

Fatty acids	Abbreviation	Pure PPFO (%)	Encapsulated PPFO (%)	Significance (<i>p</i> value)
Caprylic	C8:0	0.36 ± 0.01	0.36 ± 0.00	0.713
Capric	C10:0	0.35 ± 0.00	0.35 ± 0.00	0.815
Lauric	C12:0	6.93 ± 0.06	6.82 ± 0.04	0.071
Myristic	C14:0	3.60 ± 0.02	3.56 ± 0.02	0.099
Palmitic	C16:0	23.85 ± 0.06	23.55 ± 0.03	0.002**
Palmitoleic	C16:1 Δ ⁹	0.16 ± 0.00	0.16 ± 0.00	0.872
Stearic	C18:0	3.18 ± 0.01	3.18 ± 0.00	0.915
Oleic	C18:1 Δ ⁹	49.04 ± 0.07	48.53 ± 0.07	0.000***
<i>Cis</i> -vaccenic	C18:1 Δ ¹¹ Z	0.94 ± 0.02	0.92 ± 0.03	0.268
Linoleic	C18:2 Δ ^{9,12}	10.21 ± 0.02	10.03 ± 0.01	0.000***
Arachidic	C20:0	0.28 ± 0.00	0.28 ± 0.00	0.530
Linolenic	C18:3 Δ ^{9,12,15}	0.45 ± 0.00	0.43 ± 0.00	0.009**
<i>Cis</i> -eicosanoic	C20:1 Δ ¹¹ Z	0.15 ± 0.00	0.15 ± 0.00	0.693
Behenic	C22:0	0.10 ± 0.00	0.11 ± 0.00	0.163
Tricosanoic	C23:0	0.11 ± 0.00	0.10 ± 0.00	0.124
Lignoseric	C24:0	0.24 ± 0.00	0.23 ± 0.00	0.370
	ΣSFAs	39.00 ± 0.14	38.54 ± 0.10	0.011*
	ΣMUFAs	50.30 ± 0.10	49.76 ± 0.07	0.001*
	ΣPUFAs	10.66 ± 0.03	10.46 ± 0.01	0.000***

PPFO pressed palm fiber oil, ΣSFAs total saturated fatty acids, ΣMUFAs total monounsaturated fatty acids, ΣPUFA total polyunsaturated fatty acids

* $p < 0.05$; ** $p < 0.01$; *** $p < 0.001$

The major carotenoids in pure PPFO were β-carotene and α-carotene with concentrations of 998.31 and 635.08 μg/g oil, respectively. The same profile was observed after spray-drying; however, these compounds showed a significant but not very pronounced decrease of 8.41% (914.38 μg/g oil) and 8.54% (580.86 μg/g oil), respectively. Due to the substantial amounts of β-carotene, PPFO microparticles are good to rich sources of provitamin A.

Ferreira et al. (2016) also observed that α- and β-carotene are the main carotenoids of crude palm oil and found that, after microencapsulation by spray-drying, these compounds presented significant reduction ($p < 0.05$). These authors reported for crude and encapsulated palm oil contents of 88.78 and 67.37 μg/g oil, respectively, for all-*trans*-α-carotene and of 233.44 and 170.50 μg/g oil, respectively, for all-*trans*-β-carotene.

According to Tables 6 and 7, the pure PPFO contains high levels of unsaturated fatty acids, α- and β-carotene. In this way, PPFO is susceptible to oxidation and isomerization owing to the high number of conjugated double bonds in the chemical structure of fatty acids and carotenoids. Microencapsulation did not substantially alter the proportion between (9Z)-β-carotene isomer and all-*trans*-β-carotene (0.52 and 0.53, before and after spray-drying, respectively); however, 9-*cis*-β-carotene level was found to decrease in encapsulated PPFO. Due to the relatively high (9Z)-β-carotene content in non-encapsulated extract (522.27 μg/g oil), these results indicated that *trans-cis* isomerization and degradation of carotenoids and its *cis* isomers, during extraction and microencapsulation, can occur simultaneously in the presence of heat.

Table 7 Total carotenoids and concentrations of α-, β-, and (9Z)-β-carotene of pure and encapsulated PPFO

	Total carotenoids (μg/g oil)	α-carotene (μg/g oil)	β-carotene (μg/g oil)	(9Z)-β-carotene (μg/g oil)
PPFO	2910.55 ± 49.74	635.08 ± 16.95	998.31 ± 27.74	522.27 ± 16.56
EPPFO	2775.79 ± 124.61	580.86 ± 25.16	914.38 ± 42.40	486.14 ± 21.84
<i>p</i> value	0.052•	0.006**	0.008**	0.026*

PPFO pressed palm fiber oil, EPPFO encapsulated pressed palm fiber oil

Significance (*p* value): • $p < 0.1$; * $p < 0.05$; ** $p < 0.01$

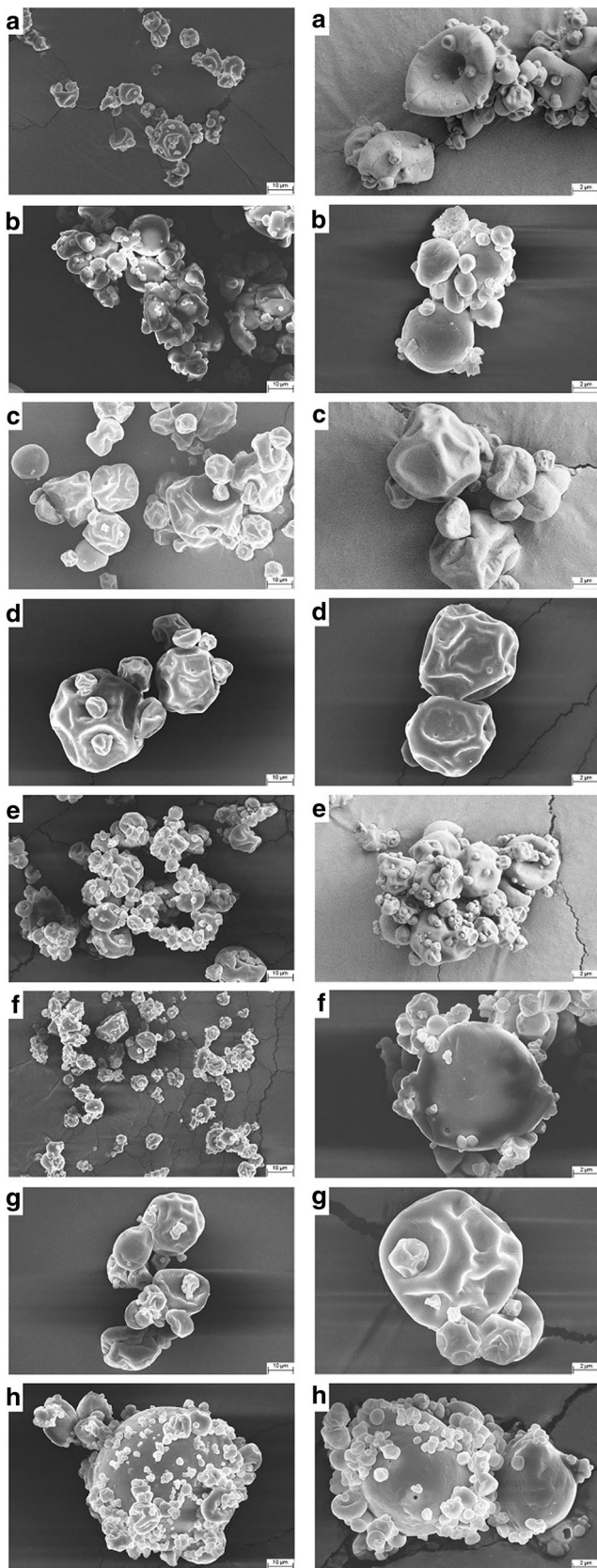


Fig. 5 Micrographs of particles with a feed flow rate of 20%, at 166 °C, atomization air flow of 40 mm, and solid contents of **a** 20 and **b** 40%; with 30% GA, at 166 °C, atomization air flow of 40 mm, and feed flow rates of **c** 8 and **d** 32%; with 30% GA, a feed flow rate of 20%, atomization air flow of 40 mm, and at temperatures of **e** 130 and **f** 202 °C; and with 30% GA, a feed flow rate of 20%, at 166 °C and atomization air flows of **g** 20 and **h** 60 mm

The high concentration of mono-*cis*- β -carotene in un-encapsulated PPFO is probably due to conversion of all-*trans*- β -carotene during the extraction, after which a decrease could occur for mono-*cis*- β -carotene because it might be further isomerized to another mono-*cis*- (difference of (9Z)- β -carotene) or di-*cis*- forms of β -carotene through intermediate all-*trans*- β -carotene or undergo degradation due to heating during microencapsulation. These results are in agreement with those observed by Lee and Chen (2002) during the study of lycopene degradation and isomerization by heating and illumination. According to these authors, once *cis* isomers are formed, a possible steric hindrance effect would be difficulty of the formation continuity of these isomers, which could be converted to other *cis*- forms.

Powder Morphology

Figure 5 shows powders' morphology produced at the axial points of the experimental design.

To gain clear insights into the surface topography, images were recorded at two different magnifications as shown in left and right micrographs. The fine cracks present on the surface observed in the larger magnification (right) were possibly formed due to the effect of electron beam irradiation. Cracks or fissures were not evident in most capsules, which imply greater retention and protection of core material against permeability to gases and oxidation reactions.

At lower GA concentration (20%, Fig. 5a), the particle appears to have more wrinkled surface, deeper cavities, and some holes (reason for the decrease in β -carotene ME—61.37%, since the uneven shrinkage might cause particle structure disruption) as opposed to the ones at higher concentration (40%, Fig. 5b) which appear more spherical and with smoother surfaces. This is due to the fact that higher solid concentrations tend to produce emulsions' much higher viscosity, which limits the droplet elasticity during drying. According to Pang et al. (2014), bubble inflation may become more prevalent at lower solid concentrations, as there is more water available to evaporate and the surface may be soft enough (due to lower solution viscosity) to allow the particle to expand. As a result, more dented surfaces are formed in the final stage of the drying process.

Particles obtained in high feed flow rates (32%, Fig. 5d) were partially collapsed, with some small pores, which may have arisen from either aeration of emulsions prior to spray-drying and/or uneven shrinkage of material during the final

drying period due to lower heat and mass transfer and, consequently, lower water evaporation rates (Ixtaina et al. 2015).

The effect of inlet air temperature on powder morphology is presented in Figs. 5e, f. When the inlet air temperature was low (130 °C), most of the particles showed a shriveled surface, while increasing drying temperatures (202 °C) resulted in a larger number of particles with rigid smooth surface and lower shrinkage. According to Tonon et al. (2008), when the drying temperature is sufficiently high, moisture is evaporated very quickly and the skin becomes dry and hard, so that the hollow particle cannot deflate when vapor condenses within the vacuole as the particle moves into cooler regions of the dryer. However, when the drying temperature is low, the skin remains moist and supple longer, so that the hollow particle can deflate and shrivel as it cools.

Particles prepared with atomization air flow of 20 mm (Fig. 5g) had deeper cavities as compared to those produced with atomization air flow of 60 mm (Fig. 5h), which resulted in microspheres with a smoother surface and fewer dent or roughness; however, it presented discontinuous walls with hole formation. These imperfections led to an ineffective protection of PPFO quality, as indicated for lower PPFO ME and the increase in PV when higher atomization air flows were used. The adherence of smaller particles on the surface of the larger ones was also observed.

Conclusions

PPFO extracted with supercritical CO₂ presented an important content of carotenoids and monounsaturated fatty acids. Higher solid content led to the formation of smaller droplets and more viscous emulsions, resulting in higher β -carotene and PPFO ME and lower peroxide value. Increasing drying temperature and feed flow rates above 26% led to an increase in PV. Higher solid concentrations combined with atomization air flow up to values around 40 mm promoted the production of powders with greater β -carotene and PPFO ME and lower peroxide values. Higher feed flow rates increased the β -carotene ME and decreased the powder hygroscopicity. Increasing temperatures and solid contents resulted in a greater number of particles with smooth surface and without cracks. Concentrations of 35% of total solids, feed flow rate of 26%, inlet air temperature of 166 °C, and atomization air flow of 40 mm were suggested as optimum conditions for PPFO spray-drying. These operating conditions preserved the carotenoids and turns PPFO microparticles into high added-value products, which can be used in the cosmetic industry, foods fortification, or as natural additives to be incorporated into food matrixes, mainly liquids, due to its contents of α - and β -carotene, attractive orange color, and hydro-solubility. Although the present results can be useful to understand the influence of emulsion properties and the effects of

operational condition on microencapsulated PPFO by spray-drying, further studies must be conducted to evaluate the influence of different types of wall materials on physicochemical properties and oxidative stability of powders during prolonged storage.

Acknowledgements The authors are grateful to CNPq (process 380344/2016-5) and Finep (project 550038/2014-0: Estratégias Genômicas e Agregação de Valor para a Cadeia Produtiva do Dendê - DendêPalm) for the financial support.

Compliance with Ethical Standards

Conflict of Interest The authors declare that they have no conflict of interest.

References

- Aghbashlo, M., Mobli, H., Madadlou, A., & Rafiee, S. (2013). Fish oil microencapsulation as influenced by spray dryer operational variables. *International Journal of Food Science and Technology*, 48(8), 1707–1713.
- Aniesrani Delfiya, D. S., Thangavel, K., Natarajan, N., Kasthuri, R., & Kailappan, R. (2015). Microencapsulation of turmeric oleoresin by spray drying and *in vitro* release studies of microcapsules. *Journal of Food Process Engineering*, 38(1), 37–48.
- AOCS. (1989). AOCS Official methods Ce 2-66 and Ce 1-62. In D. Firestone (Ed.), *Official methods and recommended practices of the American Oil Chemists's Society* (4th ed.). Champaign, IL: AOCS Press.
- Bae, E. K., & Lee, S. J. (2008). Microencapsulation of avocado oil by spray drying using whey protein and maltodextrin. *Journal of Microencapsulation*, 25(8), 549–560.
- Balasubramani, P., Palaniswamy, P. T., Visvanathan, R., Thirupathi, V., Subbarayan, A., & Prakash Maran, J. (2015). Microencapsulation of garlic oleoresin using maltodextrin as wall material by spray drying technology. *International Journal of Biological Macromolecules*, 72, 210–217.
- Bustamante, A., Masson, L., Velasco, J., del Valle, J. M., & Robert, P. (2016). Microencapsulation of *H. phuvialis* oleoresins with different fatty acid composition: kinetic stability of astaxanthin and alpha-tocopherol. *Food Chemistry*, 190, 1013–1021.
- Cardenas-Toro, F. P., Forster-Carneiro, T., Rostagno, M. A., Petenate, A. J., Maugeri Filho, F., & Meireles, M. A. A. (2014). Integrated supercritical fluid extraction and subcritical water hydrolysis for the recovery of bioactive compounds from pressed palm fiber. *The Journal of Supercritical Fluids*, 93, 42–48.
- Carneiro, H. C. F., Tonon, R. V., Grosso, C. R. F., & Hubinger, M. D. (2013). Encapsulation efficiency and oxidative stability of flaxseed oil microencapsulated by spray drying using different combinations of wall materials. *Journal of Food Engineering*, 115(4), 443–451.
- Castel, V., Rubiolo, A. C., & Carrara, C. R. (2017). Droplet size distribution, rheological behavior and stability of com oil emulsions stabilized by a novel hydrocolloid (Brea gum) compared with gum arabic. *Food Hydrocolloids*, 63, 170–177.
- Castro-Muñoz, R., Barragán-Huerta, B. E., & Yáñez-Fernández, J. (2015). Use of gelatin-maltodextrin composite as an encapsulation support for clarified juice from purple cactus pear (*Opuntia stricta*). *LWT - Food Science and Technology*, 62(1), 242–248.

- Chranioti, C., & Tzia, C. (2014). Arabic gum mixtures as encapsulating agents of freeze-dried fennel oleoresin products. *Food and Bioprocess Technology*, 7(4), 1057–1065.
- de Barros Fernandes, R. V., Marques, G. R., Borges, S. V., & Botrel, D. A. (2014). Effect of solids content and oil load on the microencapsulation process of rosemary essential oil. *Industrial Crops and Products*, 58, 173–181.
- de França, L. F., Reber, G., Meireles, M. A. A., Machado, N. T., & Brunner, G. (1999). Supercritical extraction of carotenoids and lipids from buriti (*Mauritia flexuosa*), a fruit from the Amazon region. *The Journal of Supercritical Fluids*, 14(3), 247–256.
- Deng, X.-X., Chen, Z., Huang, Q., Fu, X., & Tang, C.-H. (2014). Spray-drying microencapsulation of β -carotene by soy protein isolate and/or OSA-modified starch. *Journal of Applied Polymer Science*, 131(12), 40399–40409.
- Donhowe, E. G., & Kong, F. (2014). Beta-carotene: digestion, microencapsulation, and *in vitro* bioavailability. *Food and Bioprocess Technology*, 7(2), 338–354.
- Donhowe, E. G., Flores, F. P., Kerr, W. L., Wicker, L., & Kong, F. (2014). Characterization and *in vitro* bioavailability of β -carotene: effects of microencapsulation method and food matrix. *LWT - Food Science and Technology*, 57(1), 42–48.
- Ferreira, C. D., da Conceição, E. J. L., Machado, B. A. S., Hermes, V. S., de Oliveira Rios, A., Druzian, J. I., & Nunes, I. L. (2016). Physicochemical characterization and oxidative stability of microencapsulated crude palm oil by spray drying. *Food and Bioprocess Technology*, 9(1), 124–136.
- Frascareli, E. C., Silva, V. M., Tonon, R. V., & Hubinger, M. D. (2012). Effect of process conditions on the microencapsulation of coffee oil by spray drying. *Food and Bioprocess Technology*, 90(3), 413–424.
- Gallo, L., Llabot, J. M., Allemandi, D., Bucalá, V., & Piña, J. (2011). Influence of spray-drying operating conditions on *Rhamnus purshiana* (Cáscara sagrada) extract powder physical properties. *Powder Technology*, 208(1), 205–214.
- Gee, P. T. (2007). Analytical characteristics of crude and refined palm oil and fractions. *European Journal of Lipid Science and Technology*, 109(4), 373–379.
- Hornero-Méndez, D., Pérez-Gálvez, A., & Mínguez-Mosquera, M. I. (2001). A rapid spectrophotometric method for the determination of peroxide value in food lipids with high carotenoid content. *Journal of the American Oil Chemists' Society*, 78(11), 1151–1155.
- Ixtaina, V. Y., Julio, L. M., Wagner, J. R., Nolasco, S. M., & Tomás, M. C. (2015). Physicochemical characterization and stability of chia oil microencapsulated with sodium caseinate and lactose by spray-drying. *Powder Technology*, 271, 26–34.
- Jafari, S. M., Assadpoor, E., He, Y., & Bhandari, B. (2008). Encapsulation efficiency of food flavours and oils during spray drying. *Drying Technology*, 26(7), 816–835.
- Kha, T. C., Nguyen, M. H., Roach, P. D., & Stathopoulos, C. E. (2014). Microencapsulation of Gac oil: optimisation of spray drying conditions using response surface methodology. *Powder Technology*, 264, 298–309.
- Lee, M. T., & Chen, B. H. (2002). Stability of lycopene during heating and illumination in a model system. *Food Chemistry*, 78(4), 425–432.
- Nesterenko, A., Alric, I., Silvestre, F., & Durrieu, V. (2014). Comparative study of encapsulation of vitamins with native and modified soy protein. *Food Hydrocolloids*, 38, 172–179.
- Pang, S. F., Yusoff, M. M., & Gimbut, J. (2014). Assessment of phenolic compounds stability and retention during spray drying of *Orthosiphon stamineus* extracts. *Food Hydrocolloids*, 37, 159–165.
- Rajabi, H., Ghorbani, M., Jafari, S. M., Sadeghi Mahoonak, A., & Rajabzadeh, G. (2015). Retention of saffron bioactive components by spray drying encapsulation using maltodextrin, gum Arabic and gelatin as wall materials. *Food Hydrocolloids*, 51, 327–337.
- Rascón, M. P., Bonilla, E., García, H. S., Salgado, M. A., González-Arnao, M. T., & Beristain, C. I. (2015). T_g and a_w as criteria for the oxidative stability of spray-dried encapsulated paprika oleoresin. *European Food Research and Technology*, 241(2), 217–225.
- Rincón, S. M., & Martínez, D. M. (2009). Análisis de las propiedades del aceite de palma en el desarrollo de su industria. *Revista Palmas*, 30(2), 11–24.
- Roccia, P., Martínez, M. L., Llabot, J. M., & Ribotta, P. D. (2014). Influence of spray-drying operating conditions on sunflower oil powder qualities. *Powder Technology*, 254, 307–313.
- Rodríguez-Amaya, D. B., & Kimura, M. (2004). *HarvestPlus handbook for carotenoid analysis* (HarvestPlus Technical Monograph 2). Washington: IFPRI/CIAT.
- Rosa, M. F., Souza Filho, M. S. M., Figueiredo, M. C. B., Moraes, J. P. S., Santaella, S. T., & Leitão, R. C. (2011). Valorização de resíduos da agroindústria. II Simpósio internacional sobre gerenciamento de resíduos agropecuários e agroindustriais, Foz do Iguaçu, PR.
- Sambanthamurthiilva, R., Sundram, K., & Tan, Y.-E. (2000). Chemistry and biochemistry of palm oil. *Progress in Lipid Research*, 39(6), 507–558.
- Silva, P. I., Stringheta, P. C., Teófilo, R. F., & de Oliveira, I. R. N. (2013). Parameter optimization for spray-drying microencapsulation of jaboticaba (*Myrciaria jaboticaba*) peel extracts using simultaneous analysis of responses. *Journal of Food Engineering*, 117(4), 538–544.
- Singla, A., Ahuja, I. S., & Sethi, A. P. S. (2018). Technology push and demand pull practices for achieving sustainable development in manufacturing industries. *Journal of Manufacturing Technology Management*, 29(2), 240–272.
- Szterk, A., Roszko, M., & Górnicka, E. (2013). Chemical stability of the lipid phase in concentrated beverage emulsions colored with natural β -carotene. *Journal of the American Oil Chemists' Society*, 90(4), 483–491.
- Tonon, R. V., Brabet, C., & Hubinger, M. D. (2008). Influence of process conditions on the physicochemical properties of açai (*Euterpe oleraceae* Mart.) powder produced by spray drying. *Journal of Food Engineering*, 88(3), 411–418.
- Tonon, R. V., Grosso, C. R. F., & Hubinger, M. D. (2011). Influence of emulsion composition and inlet air temperature on the microencapsulation of flaxseed oil by spray drying. *Food Research International*, 44(1), 282–289.
- Vakili, M., Rafatullah, M., Ibrahim, M. H., Salamatinia, B., Gholami, Z., & Zwain, H. M. (2015). A review on composting of oil palm biomass. *Environment, Development and Sustainability*, 17(4), 691–709.
- Wang, R., Tian, Z., & Chen, L. (2011). A novel process for microencapsulation of fish oil with barley protein. *Food Research International*, 44(9), 2735–2741.
- Zaeim, D., Sarabi-Jamab, M., Ghorani, B., Kadkhodae, R., & Tromp, R. H. (2018). Electrospray-assisted drying of live probiotics in acacia gum microparticles matrix. *Carbohydrate Polymers*, 183, 183–191.